J. Vis. Commun. Image R. 24 (2013) 911–925

Contents lists available at SciVerse ScienceDirect

J. Vis. Commun. Image R.

journal homepage: www.elsevier.com/locate/jvci

No-reference blur image quality measure based on multiplicative multiresolution decomposition

A. Serir [a,*], A. Beghdadi [b], F. Kerouh [a]

[a] U.S.T.H.B, LTIR, Faculté d'Electronique et Informatique, Algiers, Algeria
[b] L2TI, Université Paris 13, Sorbonne Paris Cité, France

ARTICLE INFO

Article history:
Received 15 August 2012
Accepted 29 May 2013
Available online 13 June 2013

Keywords:
Blur
Contrast
Image quality
Multi-resolution analysis
MMD
Intrinsic information analysis
Support Vector Machine
Features extraction

ABSTRACT

A new approach for analyzing the blur effect on real images is proposed. This approach is based on the Multiplicative Multi-resolution Decomposition MMD. From MMD image-content analysis, a blind image quality measure dedicated to blur is then derived. The proposed measure has been applied on Gaussian-blurred and JPEG2000-compressed images from the LIVE, TID and IVC databases. The performance of the proposed measure is evaluated and compared with some referenced image quality metrics. The experimental results measured in terms of correlation with the subjective assessment of the images, demonstrate the efficiency of the proposed image quality measure in predicting the amount of blur.

© 2013 Elsevier Inc. All rights reserved.

1. Introduction

The blur is considered as one of the most studied distortions affecting image quality. It manifests itself as a loss of sharpness around edges and a decrease of visibility of fine details. This annoying degradation results from different causes. The isotropic blur effect may result from a defocus, whereas the blur due to motion appears as directional smear and contrast attenuation across contours. In microscopy blur may be due to different drifts or mechanical instabilities. The blur is often modeled through the PSF (Point Spread Function) using Linear Shift-invariant Systems theory. Many methods based on LSS theory for estimating the blur PSF without referring to the original image have been then proposed [1,17,36]. The blur could be also estimated by comparing the original images with the degraded ones using some image quality metrics. However, in many real-world applications, such as traditional television broadcast, Live Streaming and video-streaming, the original images are mostly not available. Hence, for these applications, No-Reference (NR) image quality measures are highly needed. Discriminating between image features and impairments is often ambiguous, so, quality assessment without a reference is a challenging task. However, human observer is able to discriminate between some blur effects. For example, motion produces a directional blur on the acquired images. But blur due to low pass filtering for noise reduction may appear as the blur due to lossy compression or defocusing. In this work we propose a quantitative analysis of the blur effect and propose a blurriness measure that does not make any assumption on the origin of the blur.

There are mainly two approaches for detecting and estimating the blur on images. One approach is based on the modeling of the blur effect on the image features. The second approach consists in analyzing the effect on the Human Visual System HVS [15,16,40]. Several no reference objective metrics were proposed in the literature [11]. The most known approaches are based on the analysis of the transform coefficients, such as DCT [29] or wavelet transform coefficients [2,14] or on the analysis of the edges. These approaches are based on the fact that the blur is intrinsically due to the attenuation of spatial high frequencies, which commonly occurs during image filtering or data compression. Many blur estimation methods have been proposed in the literature [4,9,12,19,25]. In contrast to other existing sharpness metrics, the metric proposed in [9] performs well under low to moderate SNR since the noise is reduced across wavelet scales. However, these approaches do not make any difference between the blur caused by compression and the one due to the image acquisition conditions.

HVS-based methods tempt to analyze the perceptual effect of the blur on the human observer. The modeling of the blur as perceived by the HVS allows to derive an objective measure directly related to the sharpness of edges and some salient features. Since edges and fine details are the most affected components by blur,

* Corresponding author.
E-mail address: aserir@usthb.dz (A. Serir).

1047-3203/$ - see front matter © 2013 Elsevier Inc. All rights reserved.
http://dx.doi.org/10.1016/j.jvcir.2013.06.002

many of the blur estimation methods are mainly based on the detection of these features. Therefore edge detection is a common step in most blurred image quality measures and several approaches have been proposed [4,5]. A blur metric defined in the spatial domain generally relies on measuring the spread of edges in an image, since blur is perceptually apparent along edges or in textured regions.

The methods described in [4,20,21,26] are performed into two main steps: edge detection and contour analysis. In the method proposed in [26] the parameters of the blur metric are tuned according to some subjective tests. Therefore, this blur measure is dependent on the test images. Furthermore, it is time consuming since it requires a search procedure to localize the extrema.

Many methods based on the modeling of the Human Visual System HVS for image analysis and processing have been proposed. One of the most studied characteristics of the HSV is its limitation to distinguish details or object on a uniform background. The notion of "just noticeable difference " (JND) [24] has been introduced in Weber-features experiment to measure the limitation of the HSV to perceive a target on a uniform background. Recently, the "just noticeable Blur" (JNB) [11] has been introduced to quantify the blurriness perception. A perceptual sharpness metric based on measured JNB and probability summation over space, which takes into account the response of the HVS to sharpness at different contrast levels, has been introduced in [11]. It provides a relative prediction of the relation sharpness/blurriness of images. Most of the aforementioned existing metrics tend to underestimate the amount of blurriness due to the fact that, at significantly high blur levels, many of the image details and edges are wiped out, which should affect the performance of the edge-based no-reference sharpness metric.

Although many interesting works on NR blur metrics have been done, there is still room for improvement. Of particular interest to this work, is to prospect new ways for analysis and assess the blurriness effect in relation with image intrinsic information modeling by using a Multiplicative Multi-resolution Decomposition [31,32] called MMD. Thus to analyze blur effect, we propose to model blurred transitions and study the polyphase components' ratio evolution close to transitions and through multi-resolution analysis.

The rest of the paper is organized as follows: blurred transitions are modeled and analyzed through multi-resolution analysis in Section 2. Then Section 3, introduces the Multiplicative Multi-resolution Decomposition. Section 4 describes the new no-reference blur quality metric. Section 5 presents the performance evaluation of the proposed method in terms of computational complexity and consistency with the subjective judgment by using LIVE, TID2008 and IVC databases. Finally, the last section is devoted to conclusion and some potential perspectives.

2. Blur analysis

The blur effect on an image could be analyzed in both the spatial or spatial-frequency domains or even in the joint space/spatial-frequency domain [3]. In the space domain the blur manifests itself as a reduction of sharpness around edges and fine details. One way for estimating the blur effect in the spatial domain is then to measure the spread of the signal around edges using some models based on the gradient measure [4,20,21,26]. In the frequency domain, the blur could be estimated by analyzing its impact on the high frequency components. Indeed, the blur distortion affects fine details and sharp transitions; this results in a decrease of the energy of high spectral components. By measuring the decrease of the energy in the frequency domain one can estimate the amount of blur [6]. Another way for characterizing the blur effect is to express the observed image using a deterministic model. One of the most used models is to consider the observed blurred image as the result of convolving the original unaltered version with the Impulse Response of a low pass filter [27]. The blur amount is then estimated through the filter parameters. Following this approach, in [8,13], the authors consider the standard deviation of the Gaussian IR as the unknown to be determined leading to estimate the strength of the blurring caused by defocusing. These methods tend to define areas with details as the sharper areas. This is not always the case since area with very few details may also look sharp. Here, we consider the underlined blurred image model to demonstrate the relevance of the multiplicative multi-resolution transform. The idea is then to model, at first, the blur effect at transitions and then, to develop suitable tools to quantify it.

To analyze the blur effect in an image I of size $K \times M$, consider the k^ith row $x(n) = I(k,n)$ with $n = 1,\ldots,M$, filtered by a one-dimensional low pass filter defined through its impulse response IR. Let us consider h this IR of length $L+1$ with $L = 2p \quad p \in \mathbb{N}$. The filtered version $x_L(n)$ could be expressed as the convolution of the original signal with h as follows:

$$x_L(n) = \sum_{l=-\frac{L}{2}}^{\frac{L}{2}} h(l)x(n+l) \tag{1}$$

Here, as an alternative to Gaussian filter we use the 1D binomial filter defined through the finite impulse response (FIR) as done in [6]. The FIR of the filter is given by:

$$h(l) = \frac{1}{2^L}\sum_{m=0}^{L} C_L^m \delta\left(l + \left(\frac{L}{2} - m\right)\right) \tag{2}$$

with $l = -\frac{L}{2},\ldots,\frac{L}{2}$. Eq. (1) could be rewritten as follows:

$$x_L(n) = \frac{1}{2^L}\sum_{m=0}^{L} C_L^m x\left(n - m + \frac{L}{2}\right) \tag{3}$$

where $C_L^m = \frac{L!}{(L-m)!m!}$.

We introduce the polyphase decomposition [37,39] which is a powerful tool for the representation of nonlinear filter banks and especially those based on the multiplicative representation.

Let us consider a signal $x(n)$. The polyphase decomposition of order N of a signal $x(n)$ involves subdividing the signal into N sub-signals $x_l(n)$ defined by (4) and illustrated in Fig. 1.

The polyphase component $x_l(n)$ is the signal $x(n)$ advanced by l and decimated by N.

$$x_l(n) = x(nN + l), \quad l \in [0 : N-1] \tag{4}$$

Let us consider $N = 2$. Thus, the polyphase components are given by:

$$\begin{aligned} x_0(n) &= x(2n) \\ x_1(n) &= x(2n+1) \end{aligned} \tag{5}$$

and those corresponding to the filtered signal are expressed as follows:

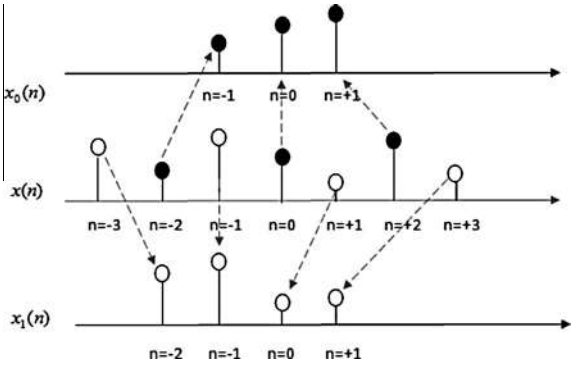

Fig. 1. Illustration of polyphase components $x_l(n)$ for $N = 2$.

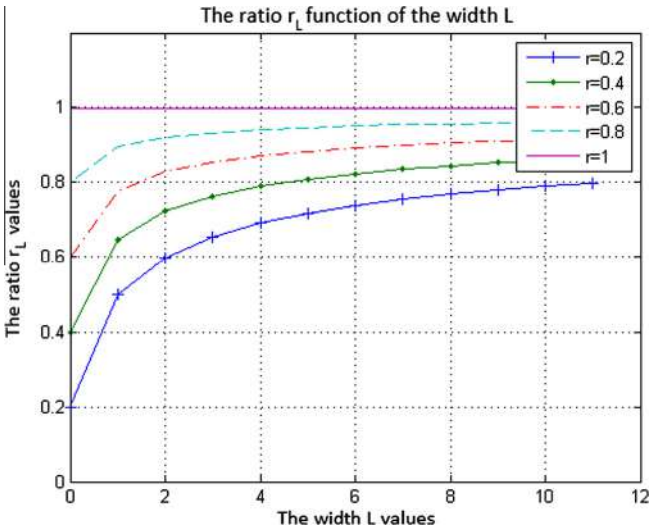

Fig. 2. The ratio r_L evolution versus the filter width L.

$$x_{L0}(n) = x_L(2n)$$
$$x_{L1}(n) = x_L(2n+1) \tag{6}$$

By using Eq. (3), the components could be rewritten as:

$$x_{L0}(n) = \frac{1}{2^L}\sum_{l=0}^{L} C_L^l \quad x\left(2n + l - \frac{L}{2}\right)$$
$$x_{L1}(n) = \frac{1}{2^L}\sum_{l=0}^{L} C_L^l \quad x\left(2n + 1 + l - \frac{L}{2}\right) \tag{7}$$

Let us assume that the k^ith row contains a transition between the positions $2n$ and $2n+1$, let say $x(2n-m) = v_1$ and $x(2n+1+m) = v_2$ with $m = 0, 1, \ldots, 2n$.

To analyze the blurring and sharpening independently from signal amplitude, let us first, consider the relative difference $d(n) = \frac{x_0(n) - x_1(n)}{x_0(n)}$ and the ratio $r(n) = \frac{x_1(n)}{x_0(n)}$, then $d(n) = 1 - r(n)$. The relative difference and the ratio of the filtered image are given by $d_L(n) = \frac{x_{L0}(n) - x_{L1}(n)}{x_{L0}(n)}$ and $r_L(n) = \frac{x_{L1}(n)}{x_{L0}(n)}$, respectively.

Thus, as

$$r(n) = \frac{x(2n+1)}{x(2n)}, \tag{8}$$

by using the Eqs. (7, 8), the blurred transition could be expressed as follows:

$$d_L(n) = 1 - r_L(n); \quad r_L(n) = \frac{(A_L + C_L^{\frac{L}{2}})r(n) + A_L}{A_L r(n) + (A_L + C_L^{\frac{L}{2}})} \tag{9}$$

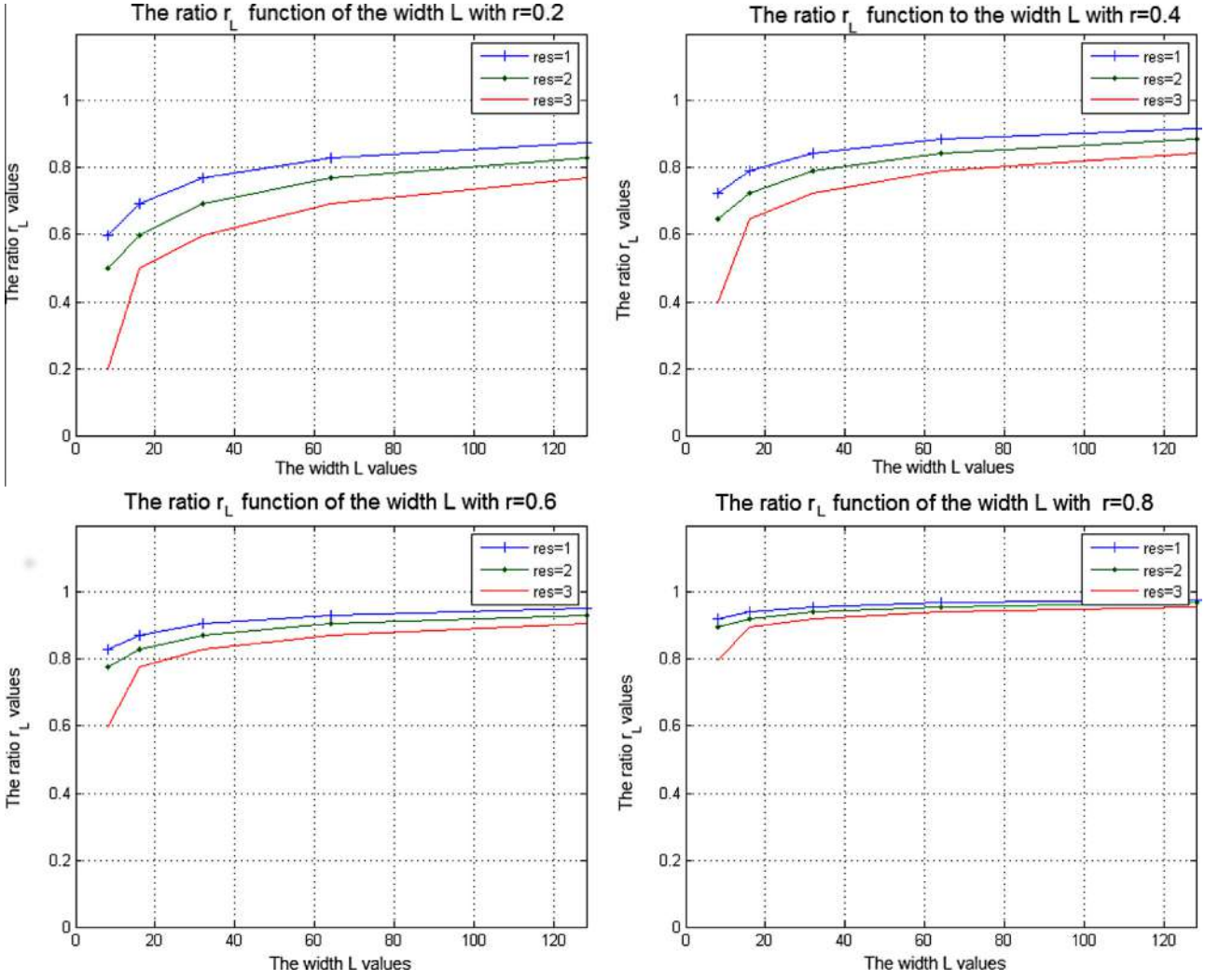

Fig. 3. The ratio r_L evolution as a function of the filter width L and the resolution j.

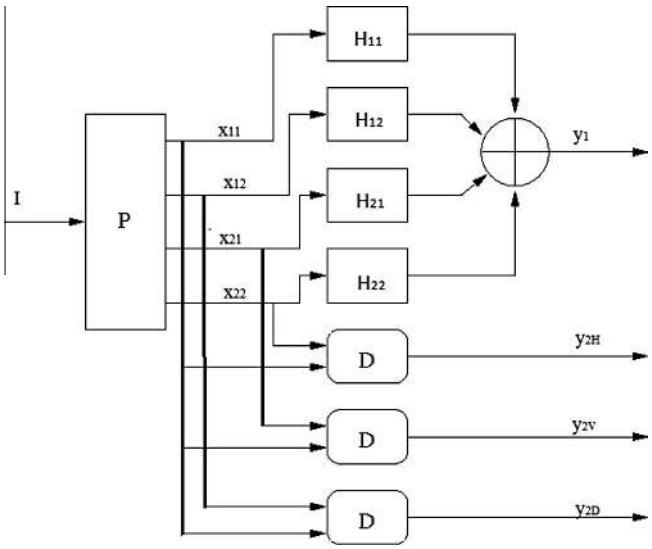

Fig. 4. The 2D MMD analysis scheme.

where

$$A_L = \sum_{u=0}^{\frac{L}{2}-1} C_L^u = \sum_{u=\frac{L}{2}+1}^{L} C_L^u; \tag{10}$$

Hence, instead of using the relative difference, the blur effect could be analyzed through the ratio $r_L(n)$. Expression (9) shows that the higher L, the greater is A_L relative to $C_L^{\frac{L}{2}}$, in this case $r_L(n) \approx 1$. For $L = 0, r_L(n) = r(n)$ since $A_L = 0$ and $C_L^{\frac{L}{2}} = 1$. Fig. 2 illustrates the evolution of $r_L(n)$ as a function of the filter width L. The curves are parameterized by the ratio $r(n)$ of the non-blurred transition. Let us consider for example $r_L(n) = 0.7$. This value could correspond to different cases $(r(n) = 0.7, L = 0)$, $(r(n) = 0.6, L = 1), (r(n) = 0.4, L = 2), \ldots$, or $(r(n) = 0.2, L = 6)$. In addition, when the transition is weak, i.e. $r(n)$ close to 1, moderate blur may yield confusion between homogeneous and inhomogeneous regions. However, when the transition is marked, such confusion may happen only in the case of strong blur.

This preliminary study shows that the ratio of signal polyphase components could be used for blurring effect analysis. More direct analysis is not sufficient to distinguish between a non-blurred, blurred non-homogeneous area and a blurred transition. Therefore, it is important to use a multi-resolution analysis by exploiting the persistence of singularities across scales. Thus, one could consider that the multi-resolution analysis is equivalent to reduce the filter width L by 2^j factor. Then the ratio r_L at the resolution j could be expressed as follows:

$$r_L^{(j)}(n) = \frac{\left(A_{\frac{L}{2^j}} + C_{\frac{L}{2^j}}^{\frac{L}{2^{j+1}}}\right) r(n) + A_{\frac{L}{2^j}}}{A_{\frac{L}{2^j}} r(n) + \left(A_{\frac{L}{2^j}} + C_{\frac{L}{2^j}}^{\frac{L}{2^{j+1}}}\right)} \tag{11}$$

Fig. 3 depicts the evolution of $r_L^{(j)}(n)$ as a function of the width L for different resolutions j and values of $r(n)$. It shows that the less original transition is marked, the less the variation of the ratio $r_L^{(j)}(n)$ within the resolutions j, is. This characteristic could be used to compute the ratio $r(n)$ corresponding to the original transition. Indeed, the ratio of the original transition could be estimated through multi-resolution analysis of $r_L^{(j)}, j = 1, 2, \ldots, J$, where $J = log_2(p)$. Furthermore, the difference $r_L^{(j)} - r_L^{(j+1)}$ is directly related to the sharpness of the original transition.

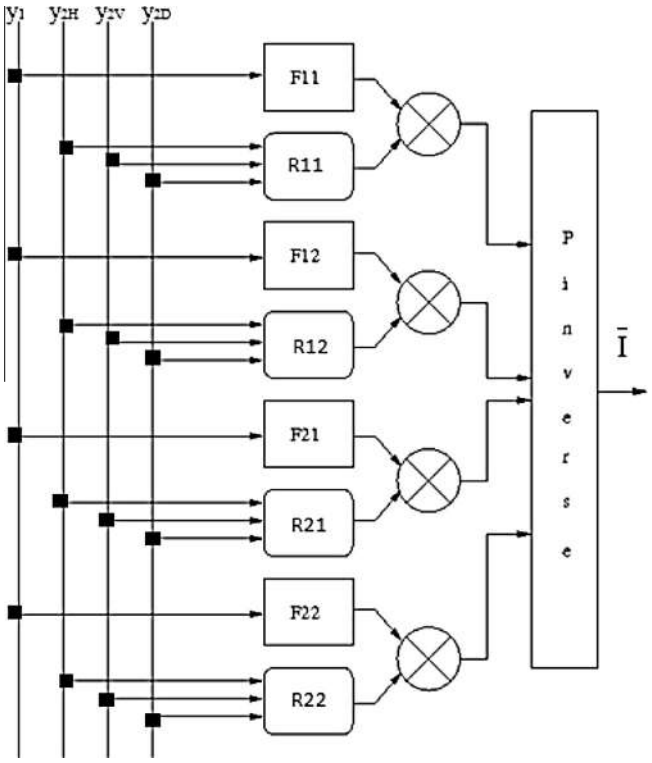

Fig. 5. The 2D MMD synthesis scheme.

3. Multiplicative multi-resolution decomposition

Through the above development, it is shown that the estimation of the ratio of polyphase components through multi-resolution analysis could be used as an efficient tool to evaluate the amount of blur in images. Therefore, one could use a multi-resolution multiplicative transform MMD [31,32], where the singularities are characterized by ratio values of polyphase components.

3.1. Multiplicative decomposition

The nonlinear multiplicative decomposition using filter banks with critical sub-sampling and perfect reconstruction [31], has been used to reduce multiplicative noise in Synthetic Aperture Radar images. The 2D extension of this transform [32] is defined as follows: let us consider a description of the analysis and synthesis one input – four output systems with equal symbol rates at both input and output. The desired structure is obtained by performing a polyphase decomposition of the 2D signal (image). The four polyphase components x_{11}, x_{12}, x_{21} and x_{22} of the input image I are defined by

$$x_{ij}(n,m) = I(2(n-1)+i, 2(m-1)+j), \quad \forall i,j \in \{1,2\}. \tag{12}$$

The proposed system requires two pairs of analysis and synthesis filters $(\{H_{ij}\}, D)$ and $(\{F_{ij}\}, R)$, respectively. A perfect reconstruction could be achieved by designing analysis $\{h_{ij}\}$ and synthesis $\{f_{ij}\}$impulse response filters satisfying the following conditions:

$$f_{ij}(k,l) = h_{ij}^{-1}(k,l), \quad i,j \in \{1,2\} \tag{13}$$

$$h_{12} = \alpha h_{11}, \quad h_{21} = \nu h_{11}, \quad h_{22} = \gamma h_{11},$$

where α, ν, γ are positive scalars and

$$h_{ij}(k,l) = h(2(k-1)+i, 2(l-1)+j), \tag{14}$$

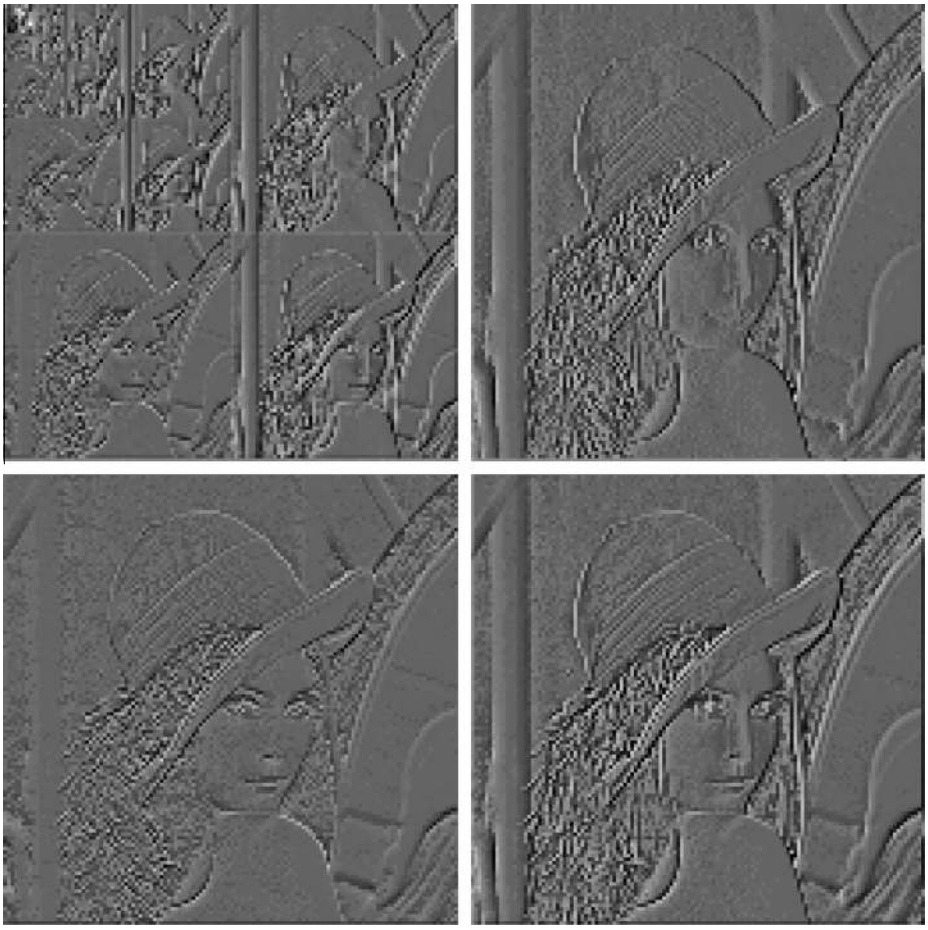

Fig. 6. 2-D MMD decomposition of Lena image at resolution 5.

$$f_{ij}(k,l) = f(2(k-1)+i, 2(l-1)+j), \quad \forall i,j \in \{1,2\}, \tag{15}$$

where h and f are bi-dimensional linear filter impulse responses.

Following the scheme (Figs. 4 and 5), the analysis and synthesis nonlinear filters $D$and R, are then specified by their input–output expressions. Thus, the nonlinear analysis filter outputs y_{2V}, y_{2H} and y_{2D} are expressed as follows:

$$y_{2V} = \begin{cases} \beta\frac{x_{12}}{x_{11}}, & x_{11} \geqslant x_{12} \\ \beta\left(2 - \frac{x_{11}}{x_{12}}\right), & x_{11} < x_{12} \\ \alpha, & x_{11} = x_{12} = 0 \end{cases} \tag{16}$$

$$y_{2H} = \begin{cases} \beta\frac{x_{21}}{x_{11}}, & x_{11} \geqslant x_{21} \\ \beta\left(2 - \frac{x_{11}}{x_{21}}\right), & x_{11} < x_{21} \\ \nu, & x_{11} = x_{21} = 0 \end{cases} \tag{17}$$

$$y_{2D} = \begin{cases} \beta\frac{x_{22}}{x_{11}}, & x_{11} \geqslant x_{22} \\ \beta\left(2 - \frac{x_{11}}{x_{22}}\right), & x_{11} < x_{22} \\ \gamma, & x_{11} = x_{22} = 0 \end{cases} \tag{18}$$

To ensure a perfect reconstruction, the synthesis nonlinear filter responses r_{ij} are derived as follows:

$$r_{11}(y_{2H}, y_{2V}, y_{2D}) = \frac{1}{1 + \alpha\psi_V + \nu\psi_H + \gamma\psi_D} \tag{19}$$

$$r_{12}(y_{2H}, y_{2V}, y_{2D}) = \alpha \times \psi_V \times r_{11}(y_{2H}, y_{2V}, y_{2D}) \tag{20}$$

$$r_{21}(y_{2H}, y_{2V}, y_{2D}) = \nu \times \psi_H \times r_{11}(y_{2H}, y_{2V}, y_{2D}) \tag{21}$$

$$r_{22}(y_{2H}, y_{2V}, y_{2D}) = \gamma \times \psi_D \times r_{11}(y_{2H}, y_{2V}, y_{2D}) \tag{22}$$

where

$$\psi_C = \begin{cases} \frac{y_{2C}}{\beta}, & y_{2C} \leqslant \beta \\ \frac{\beta}{2\beta - y_{2C}}, & y_{2C} > \beta \\ 1, & y_{2C} \in \{\alpha, \nu, \gamma\} \end{cases} \tag{23}$$

The subscript C stands for 'V', 'H' and 'D'. The parameters α, ν and γ are set to avoid singularity values so as to deal with the case where both polyphase components are null. Here, $\alpha = \nu = \gamma = 1 + \epsilon$, with ϵ very close to zero and β is set to 0.5. Thus the details y_{2H}, y_{2V}, y_{2D} vary within the interval $[0; 1 + \epsilon]$. Notice that high contrasted details correspond to values far from β. Whereas, values close to β correspond to smooth regions. Hence, for $x_{11} \neq 0$ (i.e $y_{2H} \neq \alpha, y_{2V} \neq \nu$ and $y_{2D} \neq \gamma$), according to Eqs. (16)–(18), the nonlinear response filters r_{ij} are expressed as a function of the nonlinear outputs. Following the analysis-synthesis scheme, the reconstructed polyphase components $\hat{x}_{kl}$ could be expressed as follows:

$$\hat{x}_{11} = f_{11} \times y_1 \times r_{11}(y_{2H}, y_{2V}, y_{2D}) \tag{24}$$

$$\hat{x}_{12} = f_{12} \times y_1 \times \alpha\psi_V r_{11}(y_{2H}, y_{2V}, y_{2D}) \tag{25}$$

$$\hat{x}_{21} = f_{21} \times y_1 \times \nu\psi_H r_{11}(y_{2H}, y_{2V}, y_{2D}) \tag{26}$$

$$\hat{x}_{22} = f_{22} \times y_1 \times \gamma\psi_D r_{11}(y_{2H}, y_{2V}, y_{2D}) \tag{27}$$

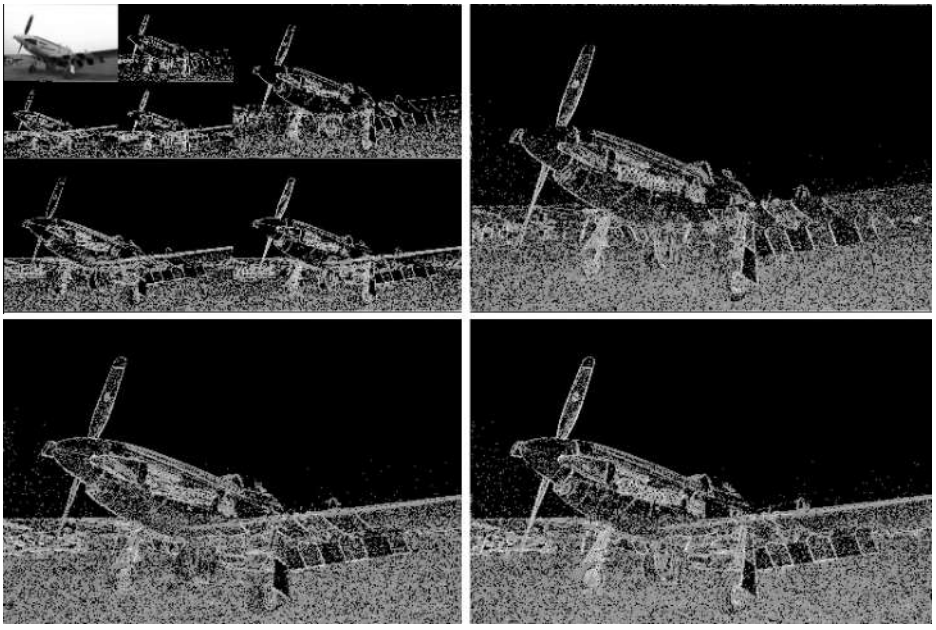

Fig. 7. 2-D MMD decomposition of an original image.

Fig. 8. 2-D MMD decomposition of a blurred image.

These equations represent the reconstructed signal as a product of a smooth component $f_{ij}.y_1$, where $y_1 = \sum_{i=1}^{2}\sum_{j=1}^{2} h_{ij}x_{ij}$, and a component containing all the signal variations expressed as localized directional ratios y_{2H}, y_{2V}, y_{2D}.

3.2. Multi-resolution multiplicative decomposition

Let us now introduce multi-resolution decomposition. It is based on sub-band decomposition using analysis filter bank that operates at different stage of the outputs. In the following, we describe the most used case where only the approximate output sub-band y_1 is decomposed into one or more coefficient outputs of the preceding stage. The sub-band y_1 is split into its polyphase components $y_{11}, y_{12}, y_{21}, y_{22}$ and then filtered. At the first resolution $j = 1$, we set $y_{11}^{(j)} = x_{11}, y_{12}^{(j)} = x_{12}$, $y_{21}^{(j)} = x_{21}$ and $y_{22}^{(j)} = x_{22}$. At the highest resolution J, the original discrete signal at the resolution 1 is represented by the set S defined by:

$$S = \left(y_1^{(J)}, \left(y_{2H}^{(j)}, y_{2V}^{(j)}, y_{2D}^{(j)}\right)_{2 \leqslant j \leqslant J}\right) \tag{28}$$

At the reconstruction stage, an approximate of the original signal at resolution $j = 1$ is obtained by using multi-resolution synthesis scheme based on the set S. Fig. 6 illustrates multiplicative multi-resolution decomposition for 5 resolution levels of *Lena* image. Fig. 6 clearly shows that the details $y_{2V}^{(j)}, y_{2H}^{(j)}$ are highlighted along the privileged direction. In the following, we will introduce a no-reference image quality index based on the multiplicative multi-resolution decomposition.

Fig. 9. The considered original images from TID2008 database.

4. A new no-reference image quality index

Image degradations, such as blurring, affect the image quality at different scale and directions. One of the most efficient way to track the distortion is to analyze the image content by using a multi-resolution representation. Indeed, multi-resolution representation offers an efficient tool for image representation and analysis. Many of the proposed image quality measures are based on multi-resolution analysis [30,40].

Through the previous analysis, it could be noticed that the two parameters $y_{2V}^{(j)}, y_{2H}^{(j)}$ contain the most relevant features of the vertical and horizontal details at the resolution j. The MMD offers an efficient tool for tracking and analyzing the effect of the blur on the spatial features of the image at different resolutions. For example, Fig. 7 shows a sharp natural image from LIVE database decomposed using a thresholded three-level MMD, while Fig. 8 shows the decomposed Gaussian blurred image. From Figs 7 and 8 , it is observed that the sharp image contains significant horizontal and vertical components in the high frequency bands; whereas the blurred image does not contain such high energy components in these bands. In smooth regions their values are close to β. As the blur effect is more apparent on image transitions, we focus on the magnitude transition analysis. Let us consider the shifted MMD coefficients given by:

$$D_C^{(j)}(n,m) = \begin{cases} 1 - y_{2C}^{(j)}(n,m) & \text{if } y_{2C}^{(j)}(n,m) < \beta \\ \beta & \text{if } y_{2C}^{(j)}(n,m) \in \{\alpha, v\} \\ y_{2C}^{(j)}(n,m) & \text{otherwise} \end{cases} \quad (29)$$

The subscript C refers to 'V', 'H' and 'D'. Hence the $D_C^{(j)}$ coefficients vary within $[0.5; 1]$.

In our approach, one could consider only the points belonging to transition and analyze the blur effect related to some image features. The image quality estimation process consists of four following steps:

1. Transition point detection.
2. Content-based image analysis.
3. Blurred transition detection.

4.1. Transition point detection

The analysis of blurred transitions through multi-resolution analysis prompts us to consider a threshold T_j , which depends on the resolution j and the intrinsic image information. Thus at each resolution j, we consider the mean values of details $m^{(j)}$ given by:

$$m^{(j)} = \frac{\overline{D_H^{(j)}} + \overline{D_V^{(j)}}}{2} \quad (30)$$

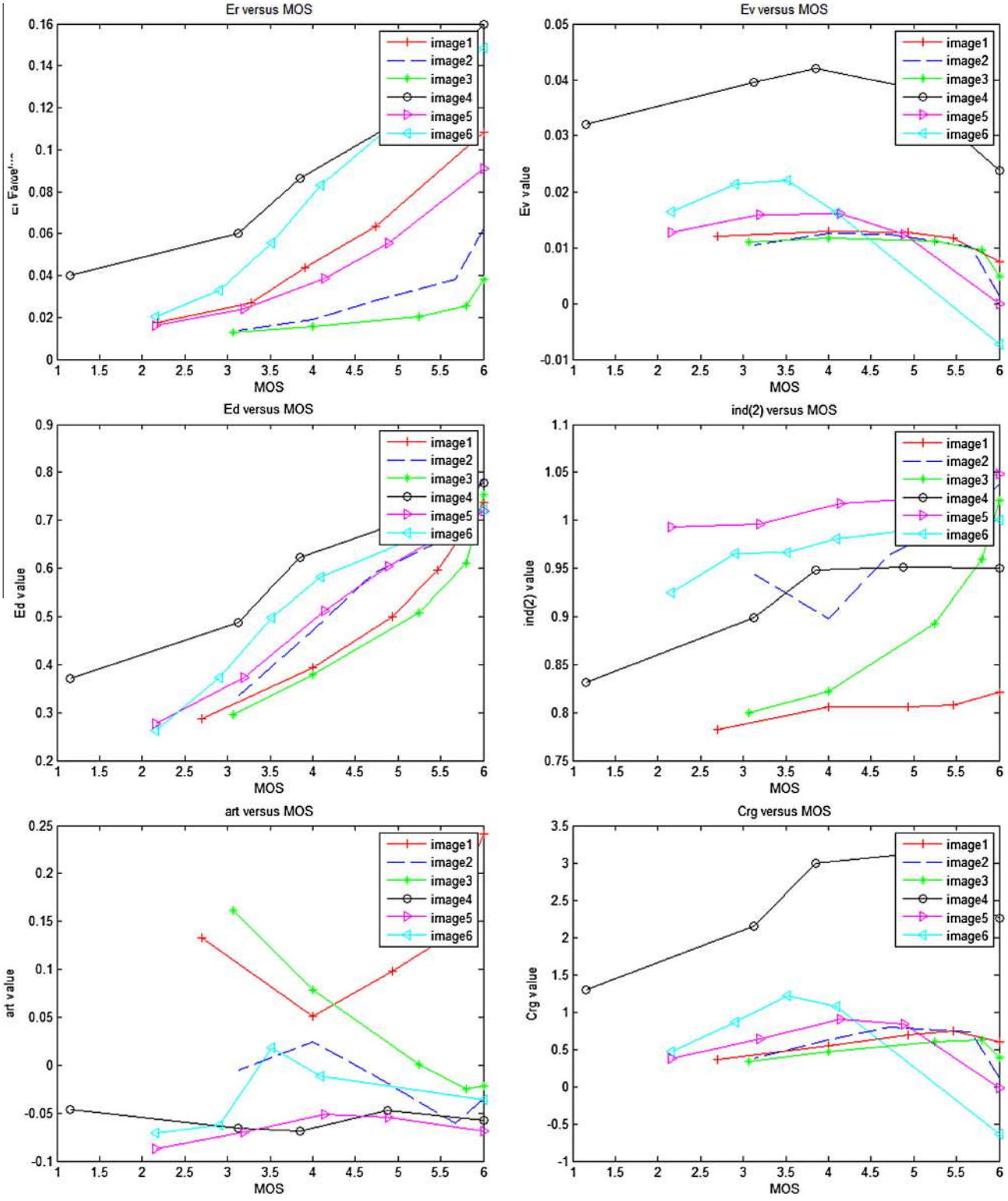

Fig. 10. Evolution of the parameters from top-left to bottom-right: $E_r, E_v, E_d, Ind^{(2)}, Art$ and Cr_g, versus MOS, for six sets of images presented in Fig. 9.

where $\overline{D_H^{(j)}}$ and $\overline{D_V^{(j)}}$ are the mean values of horizontal and vertical coefficients details $D_H^{(j)}$ and $D_V^{(j)}$, respectively. This mean value is considered as the threshold T_j for classifying transition points, $T_j = m^{(j)}$. The transition points are detected through the decision rule as follows:

$$R_C^j(n,m) = \begin{cases} D_C^j(n,m) & \text{if } D_C^j(n,m) > T_j \\ \beta & \text{otherwise} \end{cases} \tag{31}$$

4.2. Content-based image analysis

The image content as defined here is related to the following parameters:

- The structural content of the image (texture, details, contours).
- The variation of singularity magnitudes.

Table 1
Coarse classification on three classes (sharp, blurred and very blurred) by using image content information parameters.

Cases	E_r	E_v	E_d	Conditions	Observations
1	W	W	W	$Cr_g > Cr_{gs}$	Blurred
				Otherwise	Sharp
2	W	W	S	$Cr_g > Cr_{gs}$ and $Ind^{(2)} - 1 > Inds/2$	Blurred
				Otherwise	Sharp
3	W	S	W	$Art > 2Arts$	
				or $Cr_g - 1 < \frac{Cr_{gs}}{2}$ and $\lvert Ind^{(2)} - 1\rvert < Inds$	Sharp
				Otherwise	blurred
4	W	S	S	$Art \in [Arts; 2Arts]$	
				or $Cr_g - 1 < Cr_{gs}$ and	Sharp
				$\lvert Ind^{(2)} - 1\rvert < Inds$	
				Otherwise	Blurred
5	S	W	W		Sharp
6	S	W	S		Sharp
7	S	S	W	$Cr_g > 2Cr_{gs}$	Very blurred
				Otherwise	Sharp
8	S	S	S		Blurred

- The global dynamic of the singularity magnitudes or the global contrast of singularities.
- Variation of the number of contour points through resolutions.

These parameters are defined and analyzed through the transformation MMD at different levels of resolution.

The richness of the low-level texture information of a given image can be characterized by the relative difference E_r given by:

$$E_r = \frac{m^{(1)} - \beta}{\beta} \tag{32}$$

where $m^{(1)}$ stands for the average singularity magnitudes at the first resolution and β is the MMD parameter. This index provides information on the dominance of either smooth areas or textured and shape patterns in the image. Small value of E_r, correspond to an image with few singularities.

The variation of magnitude of singularities through resolutions could be characterized by the parameter E_v given by the variation of the average at the first resolution compared to the overall average $\overline{m}$:

$$E_v = \frac{\overline{m} - m^{(1)}}{\beta} \tag{33}$$

where $\overline{m} = 0.4m^{(1)} + 0.4m^{(2)} + 0.2m^{(3)}$. The number of resolutions should be set so as to achieve a trade-off between run-time and fine analysis of the edges persistence through resolutions. In this analysis three resolutions are sufficient for transition persistence analysis. The resolutions $j = 1, 2$ are more important for this purpose. Large values of E_v correspond to high sharp transitions. Whereas, low values at all resolutions correspond to persistent transitions.

The dynamic of the singularity magnitudes is given by:

$$E_d = \frac{\overline{M} - \overline{m}}{\beta}, \tag{34}$$

where $\overline{M} = 0.4M^{(1)} + 0.4M^{(2)} + 0.2M^{(3)}$ and $M^{(j)} = \max\ (\max(D_H^{(j)}), \max(D_V^{(j)}))$. E_d parameter contains amplitude variation information of the singularities and describes the sharpness in the considered image. In the case of sharp transitions, E_d takes high value.

The evolution of the number of contour points through the resolutions can be characterized by

$$Ind^{(j)} = \frac{(N_V^j + N_H^j)}{2^2(N_V^{j+1} + N_H^{j+1})}, \tag{35}$$

where N_V^j, N_H^j , are the number of vertical and horizontal transitions, respectively, at the resolution j. In the most general case, where the amount of blur present in the images is small, the number of edge points detected at resolution j is still high than at the resolution $j+1$. This is explained by the fact that the MMD performs a smoothing effect throughout the approximate component y_1. This process reduces the local transitions of roof type and noise impulse, especially in slightly blurred image. Thus, in sharp images the $Ind^{(j)}$ is always greater than 1. When it falls below 1, it means that there are transitions that were not detected at the resolution j but which may exist at the resolution $j+1$. This reflects the existence of blurred transitions considered as an homogeneous area. But they are more pronounced due to the multi-resolution analysis (sub sampling). The change in the number of contour points through resolutions, denotes information content and amount of blur present in the image. Generally the value of $Ind^{(1)}$ is still important because it marks the presence of small salient features or additive noise in the original image and the transition at resolution 1–2, reduces significantly their presence. However, in blurred images, the value of $Ind^{(1)}$ is slightly greater than 1. It may be also close to 1 if the image has well marked contours persistent through the multi-resolution analysis.

The parameter $Ind^{(2)}$ informs about the stability of the number of edges between the resolutions 2 and 3. In case of sharp and contrasted images, this index is very close to 1.

This analysis allows us to distinguish between blur due to defocussing and the localized blur effect or the artistic blur. Let us thus consider the index *Art* defined as follows:

$$Art = 1 - \frac{Ind^{(2)}}{Ind^{(1)}}. \tag{36}$$

This index is then used as a factor allowing to discriminate the localized blur or artistic blur from the global blur due to low pass filtering or motion. Indeed, for images with sharp areas, variation in the number of transition through resolutions, remains important because of the presence of fine details that progressively disappear through MMD decimation. Thus, the amount of blur in an image is related to the number of blurred contour points. Moreover, the sharpness of a given image is also related to the index *Art*. High values of *Art* correspond to high sharpness.

To illustrate how the previously introduced parameters vary with the image content and the blurriness level, we present the evolution of the parameters $E_r, E_v, E_d, Ind^{(2)}$ and *Art*, as a function of the Mean Opinion Score MOS, for six different sets of images. Each set contains an original image and its blurred versions. Fig. 9 depicts the considered original image taken from TID2008 database [28]. Fig. 10 shows that for a given image, the parameters E_r and E_d globally decrease with the MOS. The E_{r0}value in the original image depends on the structural image content (i.e texture and shape). E_{v0} values of original images are always lower than those of the corresponding blurred versions. $Ind^{(2)}$ is not close to 1 value, for very blurred images, poor-content images (for example, images 1 and 3) and images with artistic blur (example image 1). Furthermore, for these two last images, $Art \geqslant 0.1$.

Table 2
Classification rate results by considering Gblur-LIVE database, using first one parameter, then all parameters of the feature vector.

Parameter	Global rate %	Sharp %	Blur.%	Very Blur.%
E_r	71.84	76.71	80.80	42.42
E_v	64.94	56.16	85.29	42.42
E_d	45.40	52.05	30.88	60.61
$Ind^{(2)}$	47.70	52.05	30.88	72.73
Art	67.24	58.90	77.94	63.64
$\frac{Ind^{(1)}}{Ind^{(2)}}$	47.70	52.05	30.88	72.73
$\frac{Ind^{(3)}}{Ind^{(2)}}$	47.70	52.05	30.88	72.73
All	86.78	86.30	95.59	69.70

To measure the importance of parameters E_r, E_v and E_d, we have estimated them on a wide range of original images. Then we subdivide the variation domain into two regions separated by the mean value. The two regions are labeled as weak 'W' and strong 'S'. The thresholds E_{rs}, E_{vs} and E_{ds} are found approximately equal to $0.06, 0.016$ and 0.06, respectively. Thus for $E_r < E_{rs}$, the image is considered as of poor content and does not contain any significant structural information. Whereas, image transitions are analyzed through the parameters E_v and E_{vs}. Indeed, the transitions are considered as more stable through the multi-resolution analysis if E_v is less than E_{vs}. If E_d is less than E_{ds}, then the image is low contrasted. Fig. 10 shows that for original images, the parameter E_d is high. Notice that this parameter is directly related to MOS values.

One of the weaknesses of the proposed approach is that the image-content indexes are compared against fixed thresholds E_{rs}, E_{vs} and E_{ds}. For a given image, the ratio $E_r \geqslant E_{rs}$, is used as a criterion to decide whether or not the picture is rich in terms of transitions and details. However, for the sake of simplicity and without loss of generality we propose to use a global criterion Cr_g (Eq. (37)).

$$Cr_g = \frac{m^{(1)} E_v E_d}{\beta E_{vs}(\beta + E_{ds})(\beta + \beta E_{rs})}, \tag{37}$$

Fig. 10 (f) depicts the evolution of Cr_g parameter versus MOS values for different images. As Cr_g parameter depends on E_{rs}, E_{vs} and E_{ds}parameters, it is clear that the threshold value Cr_{gs} depends on the image content described by the parameter E_r. Thus in case of poor content image, Cr_{gs} could be found equal to 0.8 and in the case of rich content image, it could be set to $2.Cr_{gs}$.

In addition, one could notice that the *Art* parameter value depends on the contrast parameter E_d. For original artistic blurred images with weak contrast E_d, *Art* parameter is greater than 0.2. Whereas in the case of high value of E_d, the *Art* parameter range of variation is within the interval $[0.1; 0.2]$.

4.3. Blurred transition detection

To distinguish between blurred transitions from no blurred ones, one could take into consideration that a marked local maxima must be greater than the mean of its neighbors [7]. Let us consider local maxima $R^j_C(i,j)$ and define mean value as follows:

$$M^j_V(n,m) = \left(R^j_V(n,m+1) + R^j_V(n,m-1)\right)/2 \tag{38}$$

$$M^j_H(n,m) = \left(R^j_H(n+1,m) + R^j_H(n-1,m)\right)/2 \tag{39}$$

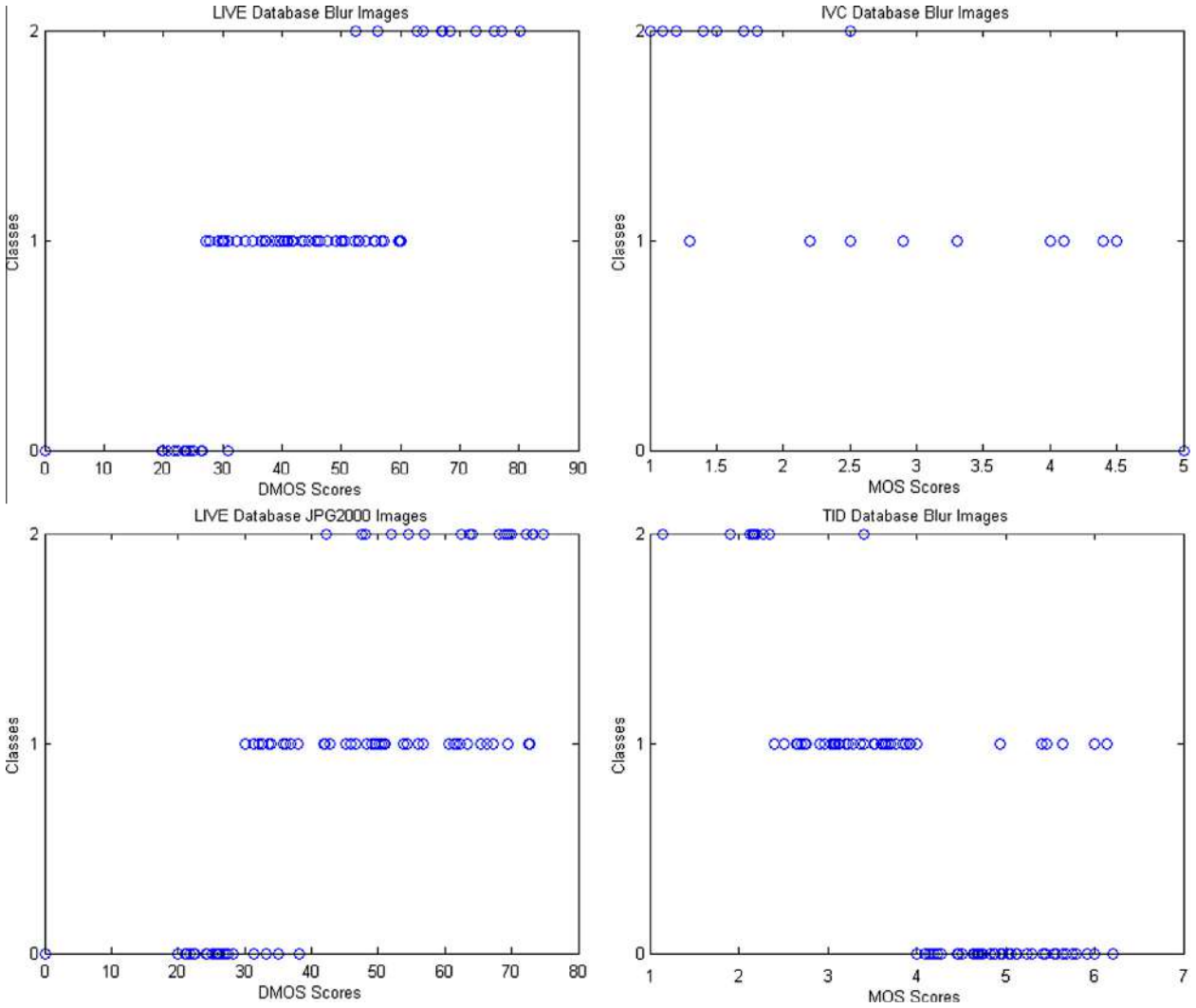

Fig. 11. Coarse classification on three groups by multi-class SVM classifier, Labels: "0" for Sharp, "1" for burred and "2" for very blurred, for the 50% samples of Gblur-LIVE and JPEG2000-LIVE databases and all samples of the IVC and TID2008 databases.

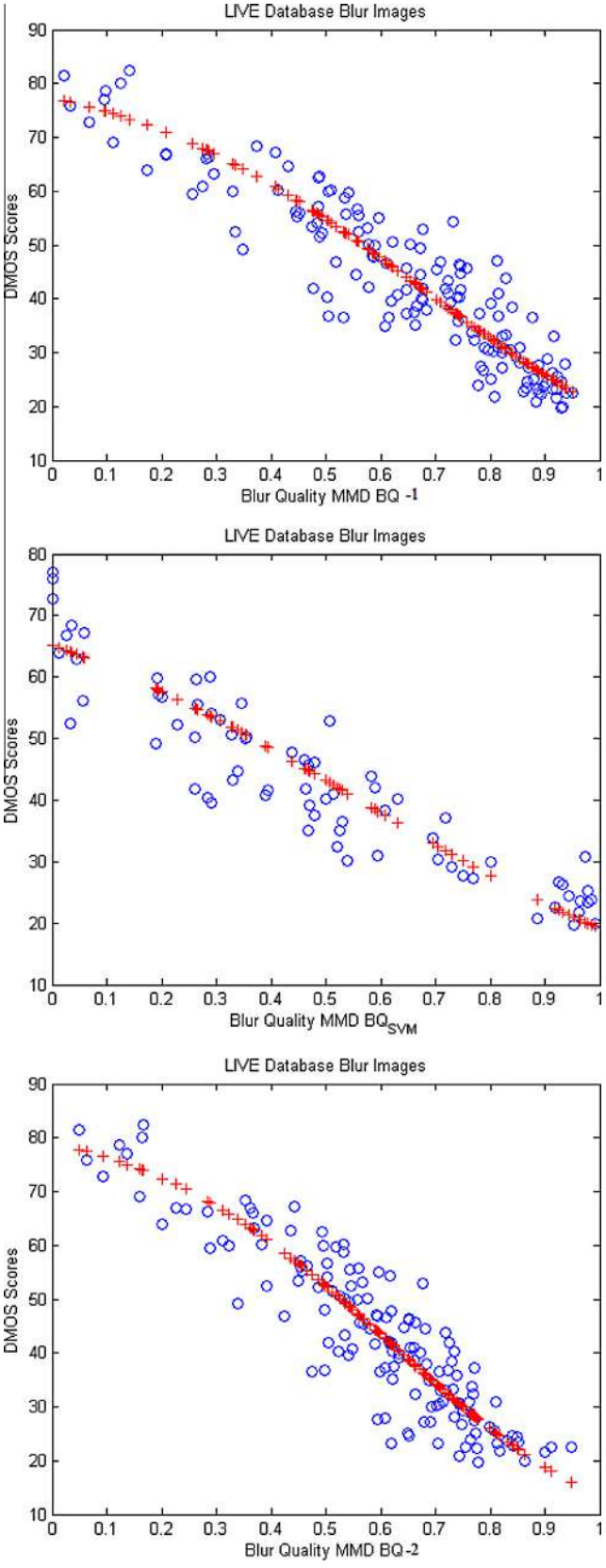

Fig. 12. Quality of blurred images by proposed metric using LIVE training images function of DMOS. From Top to bottom: direct approaches MMD-BQ-1, MMD-BQ$_{SVM}$ and iterative approach MMD-BQ-2.

Table 3
Blur Quality (BQ) performance for different no-reference algorithms applied to Gblur-LIVE database. The MMD-BQ-1 and MMD-BQ$_{SVM}$ denote the direct proposed approach based on set of thresholds and the learning based one, respectively.

Perceptual methods	SROCC	Non perceptual methods	SROCC
L. freq.[41]	0.804	QS-SVM [5]	0.6136
JNB [10]	0.71	QS-SVM DS1 [5]	0.9105
CPBD [38]	0.943	Kurtosis [4]	0,72
Marziliano [21]	0.884	Freq. thresh.[12]	0.7305
Ong [26]	0.823	NIS [9]	0.754
Chetouani [6]	0.91	MMD-BQ-1	0.9035
JNB [11]	0.936	MMD-BQ$_{SVM}$	0.9235

A given transition localized at a local maxima $\left(R_C^j(n,m) \neq \beta\right)$, is considered as sharp, if for a threshold T_s, $\left(R_C^j(n,m) - M_C^j(n,m) > T_s\right)$, otherwise, the transition at the point $(n,m)$is considered as blurred. The threshold T_s depends on the image information content which could be characterized by the parameters $E_r, E_v, E_d, Ind^{(j)}$ and *Art*. Hereafter, the threshold T_s is calculated in two steps:

- Establish a rough classification of the image on three classes (sharp, blurred and very blurred),
- calculate the threshold according to the image class.

The coarse classification could be performed by two approaches: the first is based on a set of thresholds and the second on a learning process.

4.3.1. Thresholds based approach

As discussed in Section 4.2, the content based image analysis provides a set of thresholds at which one could state that the image is of poor or rich content, the transitions are more stable through resolutions or not, that the image is poor contrasted or not and if it presents an artistic blur. Herein, we propose two approaches, namely direct and iterative approach.

Direct approach: According to the values of the indexes E_r, E_v, E_d, Cr_g, Art and $Ind^{(2)}$, the image could be classified as sharp, blurred or very blurred. For this purpose the parameters E_r, E_v and E_d are compared to the thresholds E_{rs}, E_{vs} and E_{ds}, respectively and then labeled 'W' for weak and 'S' for strong. Thus, one could identify eight possibilities summarized in Table 1. It could be noticed that the analysis of the image blurriness through the selected parameters, is facilitated in cases 5, 6 and 8. Indeed, for an image containing sharp structural transitions, the singularities vary slightly through the resolutions. If, however, they vary widely and their contrast is high, then the image is considered as blurred. In the case of highly structured images, the intrinsic information indexes or descriptors are used to raise the threshold T_s according to the strength of the richness or the variations of singularities.

Therefore, to detect blurred transitions, one could use an adaptive threshold defined by:

$$T_s = \begin{cases} T_f - \beta \frac{E_v}{m^{(1)}} & \text{sharp case} \\ T_f + \beta \frac{E_v}{m^{(1)}} & \text{blurred case} \\ T_f + \beta \frac{E_v}{m^{(1)}} + 0.01 \times Cr_g & \text{very blurred case} \end{cases} \quad (40)$$

where T_f is a fixed threshold $T_f = 0.012$. This value has been deduced from the ratio r_L evolution versus the filter width L. In the case of images with few salient structures, a special care should be taken when analyzing the spatial information. If a fixed threshold T_s= T_f is considered, the results may depend heavily on the

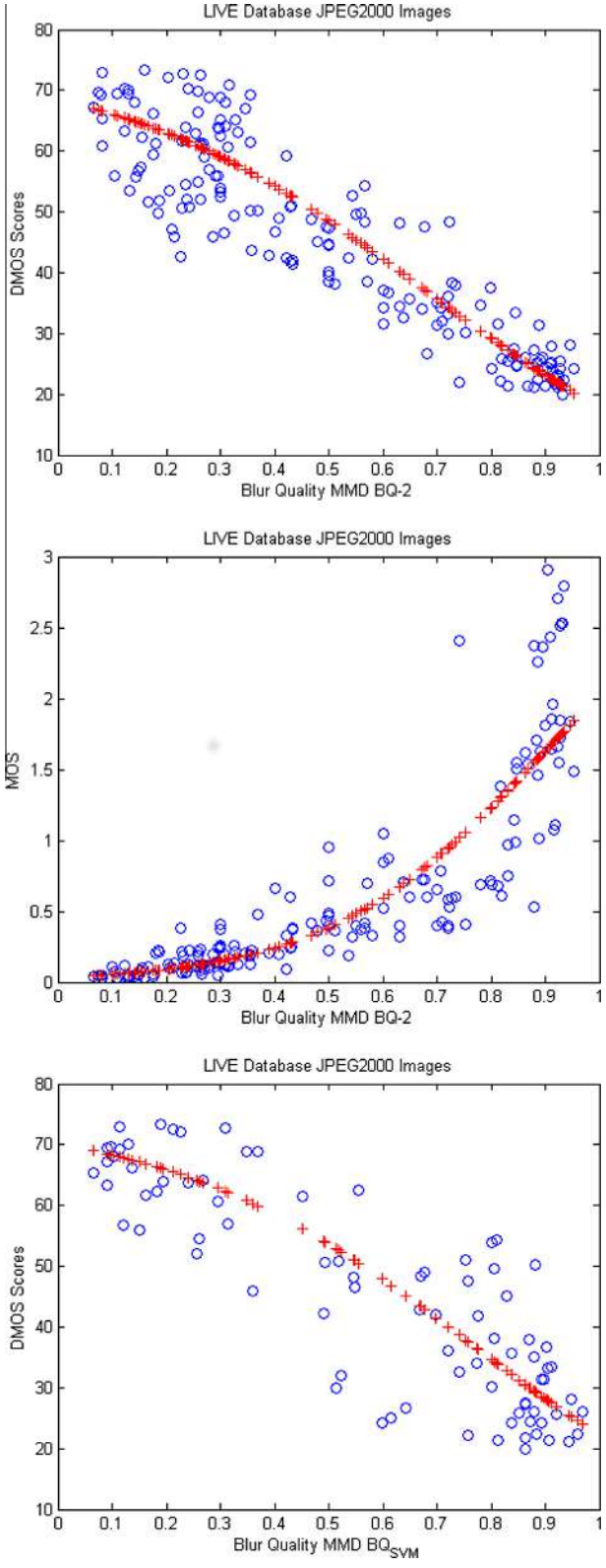

Fig. 13. Quality of JPEG2000 distorted images by proposed metric. From top to bottom: (iterative approach) using LIVE training images function of DMOS and MOS, and direct approach using learning process

choice of threshold T_f. In this work, we propose to consider an adaptive threshold controlled by image content parameters and image class deduced by a coarse classification. The fact that T_s depends on the E_v variation contributes to improve significantly the

Table 4
Blur Quality BQ performance for different no-reference algorithms applied to JPEG2000-LIVE database. The MMD-BQ-2 denotes the iterative proposed approach.

Perceptual methods	SROCC	Non perceptual methods	SROCC
JNB [11]	0.873	MMD-BQ-2	0.8877
Marziliano et al. [21]	0.782	Sazzad [30]	0.9071
Ong [26]	0.799	Sheikh [34]	0.8893

performances. In this case the aforementioned indexes allow to adjust the threshold T_s. In the case of very blurred images, the threshold T_s is adjusted according to the amount of blur by $0.01 \times Cr_g$ quantity.

Iterative approach: In this approach, the blurred transitions are detected by using an iterative thresholding scheme described below.

- Initialization: $T_s^{(0)} = T_f$ (set to a weak value).
- Iteration 1: $T_s^{(1)} = T_s^{(0)} + \frac{\beta E_v}{m^{(1)}}$
- Iteration 2: if (artistic blur: $Arts \leqslant Art \leqslant 2Arts$), then $T_s^{(2)} = T_s^{(1)}$ else $T_s^{(2)} = T_s^{(1)} + 0.02 \times Cr_g$.
- Iteration 3: if (no stability of contours through resolutions $Ind^{(2)} - 1 < Inds$ and $Art < Arts$, then $T_s^{(3)} = T_s^{(2)} + 0.02 \times Cr_g$ else $T_s^{(3)} = T_s^{(2)}$.

At each iteration the number of blurred transitions is computed. The thresholds *Arts* and *Inds* are set to 0.1 and 0.06, respectively.

The major drawback of this approach is that it depends on a set of thresholds. To evaluate the generalization of the proposed model and the robustness of its feature selection, we propose to classify the images into three groups (sharp, blurred and very blurred), by using a learning process.

4.3.2. Learning process based approach

Herein we could use the parameters E_r, E_v, E_d, $Ind^{(2)}$, $Art, \frac{Ind^{(1)}}{Ind^{(2)}}, \frac{Ind^{(3)}}{Ind^{(2)}}$ as vector features to learn a multi-class classifier. We chose to use Support Vector Machine SVM as classifier. The main reason for using SVM is that it works well for classifying a few classes with few training samples. This is highly suitable for our application were only three classes are considered. Two SVM approaches are widely used for the multi-class: One-Against-All and One-Against-One. In this work, the One-Against-All has been adopted for the multi-class SVM method, on which we fed each feature vector with its related class or label number into a multi-class SVM classifier to build the training classifier model. The label number for the training step is determined by partitioning the DMOS interval values as follows:

$$Label\ Number = \begin{cases} 0 & \text{if Dmos } < 30, \text{ sharp} \\ 1 & \text{if } 30 \leqslant \text{Dmos } < 60, \text{ blurred} \\ 2 & \text{if Dmos } \geqslant 60, \text{ very blurred} \end{cases} \quad (41)$$

Thus having a coarse classification on three groups, the threshold T_s is set as follows:

$$T_s = \begin{cases} T_f - \beta \frac{E_v}{m^{(1)}} & \text{sharp} \\ \beta \frac{E_v}{m^{(1)}} & \text{blurred} \\ T_f + \beta \frac{E_v}{m^{(1)}} & \text{very blurred} \end{cases} \quad (42)$$

The robustness of the selected image features should be shown through some classification tests in Section 5.2.1.

4.4. Blur quality estimation

To estimate the blurriness, let us consider N_{bV}^j, N_{bH}^j , the number of vertical and horizontal blurred transitions, respectively. Let us define the following factors NB^j as follows:

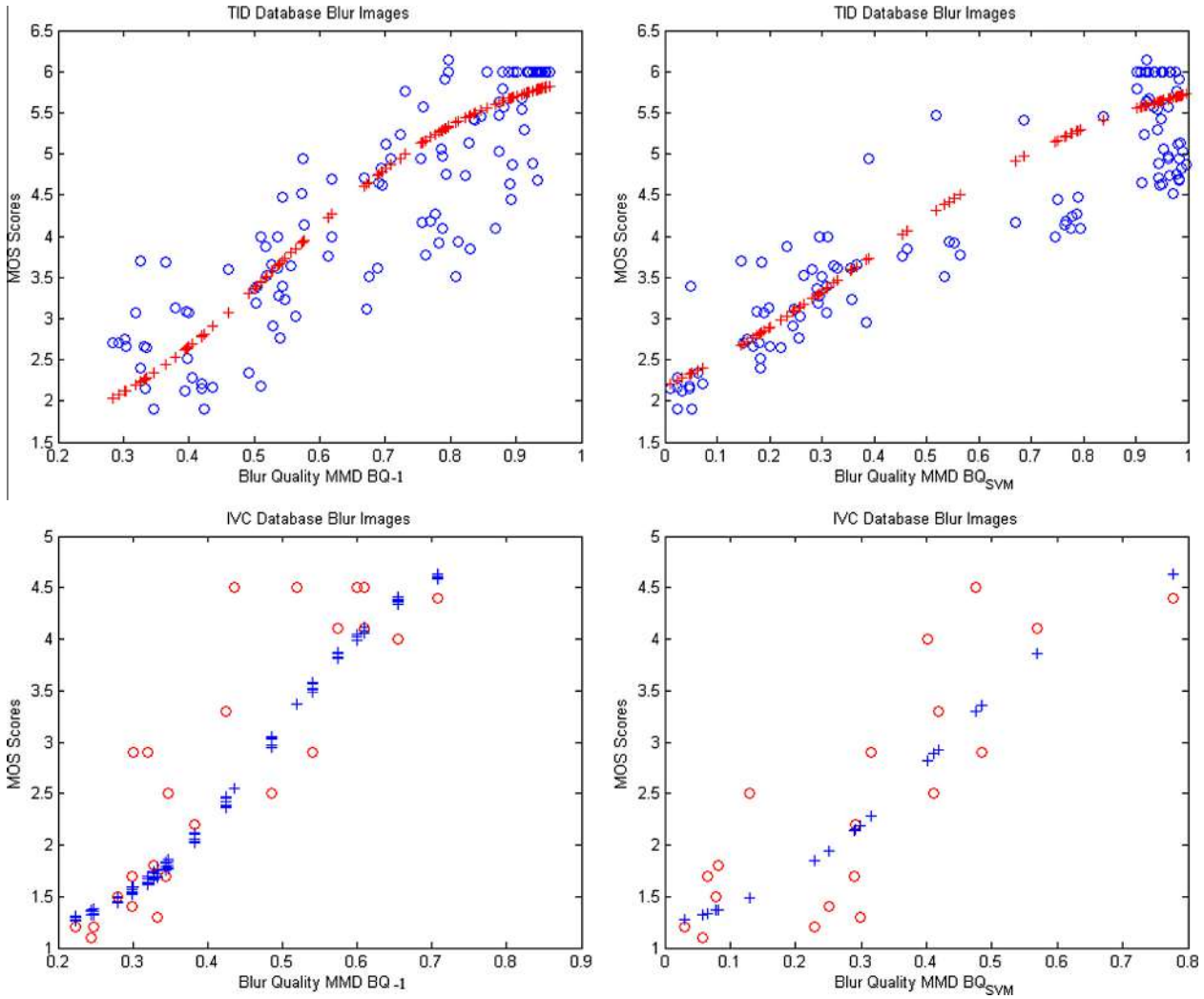

Fig. 14. Quality of blurred images by proposed metric MMD-BQ-1 and MMD-BQ$_{SVM}$ using IVC and TID training images function of MOS.

Table 5
Blur Quality BQ performance applied to TID2008 and IVC databases.

Approach	TID2008 database		IVC database	
	PCC	SROCC	PCC	SROCC
MMD-BQ-1	0.8812	0.8701	0.9124	0.8946
MMD-BQ$_{SVM}$	0.9031	0.8905	0.8480	0.8286

$$NB^{(j)} = \frac{\frac{N^j_{bV}}{N^j_V} + \frac{N^j_{bH}}{N^j_H}}{2}, \tag{43}$$

The quality of the original image in terms of blur amount is estimated as follows:

$$BQ = 1 - \frac{(4NB^{(1)} + 2NB^{(2)} + NB^{(3)})}{7}, \tag{44}$$

This scheme takes into account the spatial information content of the image and more specifically the persistence of contours across the different scales when performing the multi-resolution analysis. Moreover, in the expression (44), the quality measurements at resolution j are weighted. The weight value decreases when the resolution j increases. This is done to reduce the MMD filtering effect through this multi-resolution analysis.

In the iterative approach, the metric BQ is estimated as the mean value:

$$BQ = \frac{BQ^{(0)} + BQ^{(1)} + BQ^{(2)} + BQ^{(3)}}{4}, \tag{45}$$

where $BQ^{(k)}$ is the blur measure computed at the iteration k by using the Eq. (44). The three proposed approaches: direct, iterative (based on thresholds) and learning process based approach, are called MMD-BQ-1, MMD-BQ-2 and MMD-BQ$_{SVM}$, respectively.

5. Performance evaluation

5.1. Algorithm complexity

In this work we mainly focus on computational complexity of MMD and the parameters' computation. Let $K \times M$ be the image size. At the first resolution, the MMD decomposes image into 4 polyphase components, two of size $\frac{K}{2}$ and two of size $\frac{M}{2}$. This step is straightforward and does not cause any computation load. Then for each set of four components, four multiplications and three divisions are necessary. This results in a total of $\frac{N}{2} \times \frac{M}{2} \times 7$ operations. Then for J resolutions and taking into account the dyadic decimation, the total number of operations $Nop$is given by:

$$Nop = \sum_{j=1}^{J} \frac{7 \times K \times M}{4^j} = \frac{7}{4} \cdot \frac{1 - \left(\frac{1}{4}\right)^{(J+1)}}{1 - \frac{1}{4}} \leqslant \frac{7}{3} KM \tag{46}$$

Hence the computational complexity of the MMD is of order $O(n)$. The computation of the metric is based on the average and maximum values of MMD coefficients and the number of contour points, at each resolution. Therefore computational complexity of the image quality is of order $O(n)$.

As an example, MATLAB code takes approximately 14 s to produce a quality estimate on a 1.5 *GHz* processor with 2 *GB* of RAM running Windows XP and MATLAB R2008a, for a 512×768 image.

Note that due to the polyphase decomposition structure the method could be easily implemented on parallel architectures.

5.2. Experiment results

In this section, the obtained results are presented to illustrate the performance of the proposed blurriness metric. In this study Gaussian-blurred and JPEG2000-compressed images from the LIVE [22,23,33,35], TID [28], and IVC [18] databases are used. The main used LIVE database consists of 29 high-resolution 24-bits/pixel RGB color images. The images are distorted using different distortion types: JPEG2000, JPEG, white noise, Gaussian blur, and bit errors in the JPEG2000 bitstream when transmitted over a simulated fast-fading Raleigh channel. The Gaussian-blurred images in the LIVE database are generated using a circular-symmetric 2-D Gaussian kernel of standard deviation ranging from 0 to 15 while the JPEG2000-compressed images are generated by using a JPEG2000 software with a compression rate ranging from lossless to 0.5 bits/pixel. Performance results are presented here for both Gaussian-blurred and JPEG-2000-compressed images of the LIVE database and TID2008 and IVC databases.

5.2.1. Robustness of the selected features

The experiments were conducted first to verify the robustness of the selected image features through coarse classification process. To train the coarse multi-class SVM classifier, we used 87 training samples from Gblur-LIVE which were labeled as "sharp", "blurred" and "very blurred", by using Eq. (41). The training samples were randomly chosen. For the testing step, we have considered the remaining half of Gblur-LIVE samples and the entire IVC and TID databases. We performed the same procedure for JPEG2000-LIVE database. In order to highlight the pertinence of each image parameter, we assessed first the performance for each single parameter of the feature vector to classify the 50% of the Gblur-LIVE database. Table 2 illustrates the obtained classification rates.

One could notice that the sharp class is best characterized through parameter E_r and the blurred class by the parameters E_r, E_v and *Art*. The last class is pointed by $Ind^{(2)}$, $\frac{Ind^{(1)}}{Ind^{(2)}}$ and $\frac{Ind^{(3)}}{Ind^{(2)}}$. By using all parameters, the classification rate is about 86.78%. The Fig. 11 depicts the coarse classification by using the testing Gblur-LIVE, IVC, TID and JPEG2000-LIVE databases. The results show somehow the robustness of feature selection and the generalization of the proposed algorithm. The coarse classification rates are 91.67% for IVC, 81.45% for TID2008 and 81.42% for LIVE JPEG2000 databases.

5.2.2. Blur quality performance

To evaluate the performance of blur quality BQ, the experiments were first conducted on Gaussian-blurred images (174 images: 29 color reference images and their distorted versions using Gaussian blur) and on 227 JPEG2000-compressed images. Then, we have estimated the factor BQ for the whole considered images of LIVE database by using the direct approach with its two versions (set of thresholds based and learning process based). The variation of BQ factor versus Blur Subjective Quality BSA is represented in Fig. 12. We can notice that the factor BQ decreases inversely with the BSA factor. Less sharper the image, the higher the metric is. Thus, we have verified the validity of obtained measure using the testing images. The proposed metric provides results that are correlated well with blur subjective appreciation. A logistic function is used to adjust the objective image quality metric outputs and models it by a curve using a non-linear regression method. This regression is done by minimizing the mean square error between the proposed image quality metric measures and subjective scores. Fig. 12 illustrates these results in terms of a scatter plot with respect to subjective data. It is clearly shown that the proposed objective image quality metric is consistent with subjective evaluation.

To go one step further, the proposed metric is compared with the subjective scores provided by the LIVE DMOS. Here we restrict the study to the Spearman rank correlation coefficient (SROCC). The proposed blurriness measure is also compared with some No Reference (NR) quality measures corresponding to two approaches: perceptual and no perceptual approaches.

The considered perceptual methods are: The just noticeable blur (JNB) [10,38], frequency analysis [21,26,41] and neural based method [6].

The non perceptual methods considered here are based on the salient components of the image content such as edges [4,9,25], spatial frequency content [4]. Another approach considered in this study is based on classification scheme using Support Vector Machine [5].

Table 3 shows that among the no perceptual based methods, the direct approach based MMD-BQ-1 (quality measure based on MMD) provides relatively the best performance in terms of correlation (0.9035 for direct approach based on set of threshold and 0.9235 for direct approach based on learning process and tested on 50% of LIVE Gblur database samples).

Fig. 13 depicts the variation of BQ factor versus Blur Subjective Quality BSA applied on the overall JPEG2000-LIVE database. In [11], the results are obtained by applying the metric on 50 considered images, taken from JPEG2000-LIVE database. In order to compare the obtained results, we present the correlation results of some No Reference NR quality measures applied to JPEG2000 distorted images. The metric of [34] adopts natural scene statistics for measuring the image quality, which, however, often requires sophisticated modeling to achieve a reliable metric. A recently proposed NR metric for JPEG2000 compression [30] reports a high correlation with the LIVE database, but contains an intensive feature extraction stage (i.e., eight different spatial features) and a complex parameter optimization procedure (i.e., nine model parameters) to combine these features. Thus, our metric outperforms the alternatives of [34,30] in implementation complexity and computational efficiency. The Table 4 shows that although our metric has been applied on the overall JPEG2000 images, it provides a good performance. Herein only the iterative approach MMD-BQ-2 is considered because it depends on very few parameters. The SROCC of the metric based on direct approach using learning process and tested on 50% samples of JPEG2000-LIVE database is 0.8793.

In a second step, the proposed approaches have been applied on IVC and TID blurred databases. Fig. 14 depicts the obtained results. For evaluation criteria, we use: Pearson linear Correlation Coefficient (PCC) and Spearman Rank-Order Correlation Coefficient (SROCC). Table 5 summarizes the obtained results and shows that the latter correlated well with blur subjective appreciation.

Hence, the proposed method provides good results although it does not require any a priori knowledge on the distortion. It is worth noticing that the proposed metric could be improved by introducing a perceptual model or a classification process based

on some relevant perceptual features that could be extracted from the spatial or transform domains.

6. Conclusion

In this paper, we demonstrated a novel NR blur image quality assessment. Through Multiplicative Multi-resolution Decomposition, we find criteria to determine objective quality metric of blur effect. This metric provides an information function of blur intensity. Thus, one could easily use it, for blind image quality assessment. Three approaches are proposed, a direct approach MMD-BQ-1, an iterative approach MMD-BQ-2, all of them are based on a set of thresholds, and a learning process based approach MMD-BQ_{SVM}. The exhausted experimental results show that this method highly correlates with subjective ratings. The results show that the MMD-BQ-1 and MMD-BQ_{SVM} approaches are suitable for defocusing blur while the iterative one deals with the JPEG2000 compressed distortion. Our future work includes investigating and improving blur reduction approaches by introducing the proposed blur quality assessment metric. This could lead to define an adaptive blur reducing method.

Introducing some perceptual models for quantifying the blur effect through MM Decomposition would be also considered as a potential solution. This would undoubtedly improve the consistency of the proposed metric with the subjective evaluation.

References

[1] M.S.C. Almeida, L.B. Almeida, Blind and semi-blind deblurring of natural images, IEEE Transactions on Image Processing 19 (1) (2010) 36–52.

[2] A. Beghdadi, B. Pesquet-Popescu, A new image distortion measure based on wavelet decomposition, Signal Processing and Its Applications 1 (2003) 485–488.

[3] A. Beghdadi, R. Iordache, Image quality assessment using the joint space/spatial-frequency space, EURASIP Journal on Applied Signal Processing 2006 (2006) 8 (Article ID 80537).

[4] J. Caviedes, S. Gurbuz, No-reference sharpness metric based on local edge kurtosis, in: Proceedings of IEEE International Conference on Image Processing, vol. 1, 2002, pp. 53–56.

[5] M-J. Chen, A.C. Bovik, No-Reference image blur assessment using multiscale gradient, EURASIP Journal on Image and Video Processing, Special Issue on Quality of Multimedia Experience, January, 2011.

[6] A. Chetouani, G. Mostefaoui, A. Beghdadi, A new free reference image quality index based on perceptual blur estimation, in : PCM (IEEE Pacific Rim Conference on Multimedia) 2011, pp. 1185–1196.

[7] Min Goo Choi, Jung Hoon Jung, Jae Wook Jeon, No-reference image quality assessment using blur and noise, World Academy of Science, Engineering and Technology 50 (2009) 163–167.

[8] J.H. Elder, S.W. Zucker, Local scale control for edge detection and blur estimation, IEEE Transactions on Pattern Analysis and Machine Intelligence 20 (7) (1998) 699–716.

[9] R. Ferzli, L.J. Karam, No-reference objective wavelet based noise immune image sharpness metric, in: IEEE International Conference on Image Processing, 2005, pp. 405–408.

[10] R. Ferzli, L.J. Karam, A human visual system based on reference objective image sharpness metric, in: IEEE International Conference on Image Processing, pp. 2949–2952, 2006.

[11] R. Ferzli, L.J. Karam, A no-reference objective image sharpness metric based on the notion of just noticeable blur (JNB), IEEE Transaction on Image Processing 18 (4) (2009) 717–728.

[12] L. Firestone, K. Cook, N. Talsania, K. Preston, Comparison of autofocus methods of automated microscopy, Cytometry 12 (1991) 195–206.

[13] H. Hu, G.D. Haan, Low cost robust blur estimation, in: Proceedings of IEEE International Conference on Image Processing, 2006.

[14] R. Hassen, Z. Wang, M. Salama, No-reference image sharpness assessment based on local phase coherence measurement, in: Proceedings of IEEE International Conference on Acoustics, Speech & Signal Processing, 2010.

[15] J. Jayant, J. Johnston, R. Safranek, Signal compression based on models of human perception, Proceedings of the IEEE 81 (10) (1993) 1385–1422.

[16] L.J. Karam, T. Ebrahimi, S. Hemami, T. Pappas, B. Saframeh, Z. Wang, A.B. Watson, Introduction to the Issue on Visual Media Quality Assessment, IEEE Journal on Selected Topics in Signal Processing (Special Issue on Visual Media Quality Assessment) 3 (2) (2009) 189–192.

[17] D. Kundur, D. Hatzinakos, Blind image deconvolution, IEEE Signal Processing Magazine 13 (3) (1996) 43–64.

[18] P. Le Callet, F. Autrusseau, "Subjective quality assessment IRCCyN/IVC database", 2005.

[19] X. Marichal, M. Wei-Ying, H.J. Zhang, Blur dertermination in the compressed domain using DCT information, in: Proceedings of IEEE International Conference on Image Processing, vol. 3, 1999, pp. 386–390

[20] P. Marziliano, F. Dufaux, S. Winkle, T. Ebrahimi, A no-reference perceptual blur metric, in: Proceedings of IEEE International Conference on Image Processing, vol. 3, 2002, pp. 57–60

[21] P. Marziliano, S. Winkler, F. Dufaux, T. Ebrahimi, Perceptual blur and ringing metrics: application to JPEG2000, Elsevier Signal Processing : Image Communication 19 (2) (2004) 163–172.

[22] A.K. Moorthly, K. Seshadrinathan, R. Soundararajan, A.C. Bovik, Wireless video quality assessment: a study of subjective scores and objective algorithms, IEEE Transactions on Circuits and Systems for Video Technology 20 (4) (April 2010) 587–599.

[23] A.K. Moorthly, A.C. Bovik, A two-step framework for constructing blind image quality indices, IEEE Signal Processing Letters 17 (5) (2010) 513–516.

[24] A.K. Moorthly, A.C. Bovik, Blind image quality assessment: from natural scene statistics to perceptual quality, IEEE Transactions on Image Processing 20 (12) (2011) 3350–3364.

[25] R.B. Nill, B.H. Bouzas, Objective image quality measure derived from digital image power spectra, Optical Engineering 31 (4) (1992) 813–825I.

[26] E. Ong, W. Lin, Z. Lu, S. Yao, X. Yang, L. Jiang, A no-reference quality metric for measuring image blur, in: Proceedings of International Conf. Image Processing, 2003, pp. 469–472.

[27] A. Pentland, T. Darrell, M. Turk, W. Huang, " A simple real time range camera, in: IEEE Computer Society Conference on Computer Vision and Pattern Recognition, 1989, pp. 256–261.

[28] N. Ponomarenko, V. Lukin, A. Zelensky, K. Egiazarian, M. Carli, F. Battisti, TID2008 – a database for evaluation of full-reference visual quality assessment metrics, Advances of Modern Radioelectronics 10 (2009) 30–45.

[29] M.A. Saad, A.C. Bovik, C. Charrier, Natural DCT Statistics Approach to no-reference image quality assessment, in: IEEE International Conference on Image Processing, 2010.

[30] Z. Sazzad, Y. Kawayoke, Y. Horita, No reference image quality assessment for JPEG2000 based on spatial features, Signal Processing Image Communication 23 (2008) 257–268.

[31] A. Serir, A. Belouchrani, Multiplicatif multiresolution decomposition with perfect reconstruction, in: IEEE ISSPIT, Darmstadt, Allemagne, 14–17 Décembre, 2003.

[32] A. Serir, A. Belouchrani, Multiplicatif multiresolution Decomposition for 2D signals: application to speckel reduction in SAR images, in: IEEE International Conference on Image Processing, october, 2004, pp. 24–25.

[33] H.R. Sheikh, Z. Wang, L. Cormack, A.C. Bovik, LIVE image quality assessment database release 2. <http://live.ece.ute.xas.edu/research/quality>.

[34] H.R. Sheikh, A.C. Bovik, L.K. Cormack, No-reference quality assessment using natural scene statistics: JPEG2000, IEEE Transactions on Image Processing 14 (11) (2005) 1918–1927.

[35] H.R. Sheikh, M.F. Sabir, A.C. Bovik, A statistical evaluation of recent full reference image quality assessment algorithms, IEEE Transactions on Image Processing 15 (11) (2006) 3440–3451.

[36] W. Souidene, K. Abed-Meraim, A. Beghdadi, A new look to Multichannel Blind Image Deconvolution, IEEE Transactions on Image Processing 18 (7) (2009) 1487–1500.

[37] P.P. Vaidyanathan, Multirate digital filters, filter banks, polyphase networks, and applications: A tutorial, Proceedings of the IEEE 78 (1) (1990).

[38] S. Varadarjan, L.J. Karam, An improvment perception based no reference objective image sharpness metric using iterative edge refinement, in: International Conference on Image Processing, 2008, pp. 401–404.

[39] M. Vetterli, A theory of multirate filter banks, IEEE Transactions on Acoustics, Speech and Signal Processing ASSP-35 (3) (1987).

[40] Z. Wang, A.C. Bovik, H.R. Sheikh, E.P. Simoncelli, Image quality assessment: from error visibility to structural similarity, IEEE Transactions on Image Processing 113 (4) (April. 2004) 600–612.

[41] Z. Wang, A.C. Bovik, Modern Image Quality Assessment, Morgan & Claypool Publishers, 2006.